

Sampling-Based Accuracy Testing of Posterior Estimators for General Inference

Pablo Lemos^{1 2 3 4*} Adam Coogan^{1 2 3*} Yashar Hezaveh^{1 2 3} Laurence Perreault-Levasseur^{1 2 3}

Abstract

Parameter inference, i.e. inferring the posterior distribution of the parameters of a statistical model given some data, is a central problem to many scientific disciplines. Posterior inference with generative models is an alternative to methods such as Markov Chain Monte Carlo, both for likelihood-based and simulation-based inference. However, assessing the accuracy of posteriors encoded in generative models is not straightforward. In this paper, we introduce ‘distance to random point’ (DRP) coverage testing as a method to estimate coverage probabilities of generative posterior estimators. Our method differs from previously-existing coverage-based methods, which require posterior evaluations. We prove that our approach is necessary and sufficient to show that a posterior estimator is optimal. We demonstrate the method on a variety of synthetic examples, and show that DRP can be used to test the results of posterior inference analyses in high-dimensional spaces. We also show that our method can detect non-optimal inferences in cases where existing methods fail.

1. Introduction

In scientific analyses, determining the values of unknown parameters θ in a statistical model given observed data x , known as parameter inference, is a ubiquitous task. While multiple approaches exist, such as Markov-Chain Monte Carlo (MCMC) and variational inference (VI), there has been a recent shift in many scientific fields towards using machine learning for amortized posterior inference (e.g. [Zhu & Zabaras, 2018](#); [Papernot & McDaniel, 2018](#); [Charnock et al., 2020](#); [Wilson & Izmailov, 2020](#); [Zuo et al., 2020](#)). This approach involves training a model, typically a neural network, to approximate the true posterior distribution by minimizing the difference between the estimated and desired posterior distribution. The goal is to efficiently estimate the posterior for new data points, eliminating the need for using costly MCMC or VI methods for every additional observation.

Simulation-based inference (SBI, e.g. [Cranmer et al., 2020](#)),

also known as likelihood-free inference (LFI) or implicit likelihood inference (ILI), has gained significant popularity in recent years (e.g. [Ong et al., 2018](#); [Perreault Levasseur et al., 2017](#); [Gonçalves et al., 2020](#); [Dax et al., 2021](#); [Alsing et al., 2019](#); [Wagner-Carena et al., 2021](#); [Legin et al., 2021](#); [Brehmer, 2021](#); [Coogan et al., 2020](#); [Montel et al., 2022](#); [Coogan et al., 2022](#); [Brehmer et al., 2019](#); [Mishra-Sharma & Cranmer, 2022](#); [Karchev et al., 2022b](#); [Hermans et al., 2021a](#); [Anau Montel & Weniger, 2022](#); [de Witt et al., 2020](#); [Marlier et al., 2021](#); [Karchev et al., 2022a](#); [Ramesh et al., 2022](#)). SBI does not require an explicit expression for the likelihood, and instead merely relies on having a simulator to generate training data. The SBI framework allows handling complex, high-dimensional data and models that are difficult or intractable to analyze using traditional likelihood-based methods.

Early developments of SBI include the introduction of Rejection Approximate Bayesian Computation (ABC) ([Rubin, 1984](#); [Pritchard et al., 1999](#); [Beaumont et al., 2002](#); [Marjoram et al., 2003](#); [Fearnhead & Prangle, 2012](#)), but today SBI has evolved to encompass more powerful, neural network-powered, amortized methods, such as Neural Ratio Estimation (NRE) ([Cranmer et al., 2015](#); [Thomas et al., 2022](#); [Hermans et al., 2020](#); [Durkan et al., 2020](#); [Miller et al., 2022b](#)); Neural Posterior Estimation (NPE) ([Rezende & Mohamed, 2015](#); [Papamakarios & Murray, 2016](#); [Lueckmann et al., 2018](#); [Lueckmann et al., 2017](#); [Greenberg et al., 2019](#)) and Neural Likelihood Estimation (NLE) ([Price et al., 2018](#); [Papamakarios et al., 2019](#); [Frazier et al., 2022](#)). Recently there has been substantial interest in applying SBI in high-dimensional parameter spaces. Generative models, such as Generative Adversarial Networks ([Goodfellow et al., 2014](#)), Normalizing Flows ([Dinh et al., 2014](#); [Rezende & Mohamed, 2015](#); [Papamakarios et al., 2021](#)), Variational Autoencoders ([Kingma & Welling, 2013](#)) and Score-Based/Diffusion Models ([Song et al., 2020](#); [Ho et al., 2020](#); [Sohl-Dickstein et al., 2015](#)), are a useful way to encode approximate posteriors in such settings.

Accuracy tests for MCMC methods are well established, and there are many metrics to evaluate the quality of the posterior distributions, such as the Gelman-Rubin statistic ([Gelman & Rubin, 1992](#)), the effective sample size, and the integrated autocorrelation time. For SBI, testing for accuracy of the

estimated posterior is often performed using coverage probabilities (but see also [Guo et al. \(2017\)](#)), relying on the evaluation of the density of the posteriors. ([Schall, 2012](#); [Prangle et al., 2013](#); [Cranmer et al., 2020](#); [Hermans et al., 2021b](#)). Coverage probabilities measure the proportion of the time that a certain interval contains the true parameter value. However, coverage probability calculations based on evaluations of the learned posterior distributions are not applicable to samples obtained from a generative model, where such evaluations are not available. Furthermore, and more importantly, these coverage probabilities tests are a necessary but not sufficient diagnostic to assess the accuracy of the estimated posterior.

Although other works have suggested alternative validation methods for SBI ([Talts et al., 2018](#); [Lueckmann et al., 2021](#); [Dalmasso et al., 2020](#); [Linhart et al., 2022](#); [Deistler et al., 2022](#)), none of these can be applied for generative models on arbitrary dimensions when we do not have access to posterior evaluations.

The goal of this paper is to introduce a framework for testing the accuracy of parameter inference using only samples from the true joint distribution of the data x and the parameters of interest θ , $p(x, \theta)$, and samples from the estimated posterior distribution $\hat{p}(\theta|x)$. We begin by introducing all necessary notation in §2. We then introduce our method in §3. We present our experiments in §4, and summarize our findings in §5. An example implementation of our code is available upon request.

2. Formalism

In this section, we introduce some basic concepts and build up to our key theoretical result (Theorem 3). The coverage testing procedure introduced in the following section is essentially a practical implementation of this theorem.

2.1. Notation

As stated in the introduction, we are interested continuous-valued parameters $\theta \in U \subset \mathbb{R}^n$ and observations $x \in V \subset \mathbb{R}^m$ taken from (subsets of) Euclidean space, with joint density $p(\theta, x)$. We denote our posterior estimator by $\hat{p}(\theta|x)$ (which could be a neural network or MCMC sampler, for example) and assume we can also use it to generate samples of θ .

With these preliminaries, we make two basic definitions:

Definition 1. A posterior estimator $\hat{p}(\theta|x)$ is **optimal** if

$$\hat{p}(\theta|x) = p(\theta|x) \quad \forall (x, \theta) \sim p(x, \theta). \quad (1)$$

Definition 2. A **credible region generator** $\mathcal{G} : \hat{p}, \alpha, x \mapsto W \subset U$ for a given credibility level α and observation x is

a function satisfying

$$\int_{\mathcal{G}(\hat{p}, \alpha, x)} d\theta \hat{p}(\theta|x) = 1 - \alpha. \quad (2)$$

Note that there are an infinite number of such generators. A commonly-used one is the highest-posterior density region generator, which produces the region with mass $1 - \alpha$ occupying the smallest-possible volume in U ¹.

Next, we introduce two central definitions for this work, adapted from [Hermans et al. \(2021b\)](#) (henceforth H21).

Definition 3. The **coverage probability** for a generator \mathcal{G} , credibility level α and datum x is

$$CP(\hat{p}, \alpha, x, \mathcal{G}) = \mathbb{E}_{p(\theta|x)} [\mathbb{1}(\theta \in \mathcal{G}(\hat{p}, \alpha, x))]. \quad (3)$$

Definition 4. The **expected coverage probability** for a generator \mathcal{G} and credibility level α is the coverage probability averaged over the data distribution:

$$ECP(\hat{p}, \alpha, \mathcal{G}) = \mathbb{E}_{p(x)} [CP(\hat{p}, \alpha, x, \mathcal{G})]. \quad (4)$$

2.2. Coverage probability

We now demonstrate some basic facts about estimators with correct coverage probabilities. We begin with a straightforward result:

Theorem 1. The posterior has coverage probability $CP(p, \alpha, x, \mathcal{G}) = 1 - \alpha$ for all values of x and any credible region generator $\mathcal{G}(\hat{p}, \alpha, x)$.

Proof Substituting $\hat{p}(\theta|x) = p(\theta|x)$, the definition of coverage probability becomes:

$$\begin{aligned} CP(p, \alpha, x, \mathcal{G}) &= \mathbb{E}_{p(\theta|x)} [\mathbb{1}(\theta \in \mathcal{G}(p, \alpha, x))] \\ &= \int_{\mathcal{G}(p, \alpha, x)} d\theta p(\theta|x) \\ &= 1 - \alpha, \end{aligned} \quad (5)$$

where the last line follows from the definition of a credible region. ■

It follows trivially from this that the posterior has $ECP(p, \alpha, x, \mathcal{G}) = 1 - \alpha$ as well.

Next, we prove the more interesting reverse direction of this theorem. To do this we introduce the concept of a *positionable credible region generator* $\mathcal{P}_{\theta_r}(\hat{p}, \alpha, x)$ that generates credible regions positioned at θ_r . Technically, this means $\lim_{\alpha \rightarrow 1} \mathcal{P}_{\theta_r}(\hat{p}, \alpha, x) = \mathbb{1}(\theta = \theta_r)$ for all x and θ_r . The regions' shapes are not important: they could be, for example, balls or hypercubes. We also define the average of a function $f(\theta)$ over a credible region Θ positioned at θ_r as

$$\overline{f(\cdot)}(\Theta) := \frac{1}{\text{vol}[\Theta]} \int_{\Theta} d\theta f(\theta). \quad (6)$$

¹Note this is ill-defined for the uniform density function.

This is itself a probability density function over θ_r .

Theorem 2. Suppose the coverage probability of a posterior estimator is equal to $1 - \alpha$ for a positionable credible region generator \mathcal{P}_{θ_r} for all θ_r , x and α . Further, suppose that $\hat{p}(\cdot|x)$ has support everywhere in the parameter space for all x . Then $\hat{p}(\cdot|x) = p(\cdot|x)$.

Proof Define $\Theta := \mathcal{P}_{\theta_r}(\hat{p}, \alpha, x)$ for clarity.

The integral in the definition of the coverage probability can be written as

$$\begin{aligned} \text{CP}(\hat{p}, \alpha, x, \mathcal{P}_{\theta_r}) &= 1 - \alpha \\ &= \int_{\Theta} d\theta \hat{p}(\theta|x) \\ &= \text{vol}[\Theta] \overline{\hat{p}(\cdot|x)}(\Theta), \end{aligned} \quad (7)$$

where first equality follows by assumption. Since we've assumed $\hat{p}(\cdot|x)$ has support everywhere, the volume of the credible region is positive. By the definition of a credible region, we also have

$$1 - \alpha = \int_{\Theta} d\theta \hat{p}(\theta|x) = \text{vol}[\Theta] \overline{\hat{p}(\cdot|x)}(\Theta). \quad (8)$$

Setting this equal to the previous expression yields $\overline{\hat{p}(\cdot|x)}(\Theta) = \overline{p(\cdot|x)}(\Theta)$, which holds for all θ_r and x by assumption. Taking $\alpha \rightarrow 1$ (i.e., making Θ small) gives the desired result. \blacksquare

2.3. Expected coverage probability

The previous result is still not very useful, since it is computationally very expensive to calculate the coverage probability of a posterior estimator. Practically, doing so requires producing histograms of the samples from $p(\theta, x)$ in x , which may be high-dimensional. However, as pointed out in H21, it's much simpler to compute the *expected* coverage probability.

The next theorem is our main theoretical result: correct expected coverage is enough to verify the posterior estimator is optimal, as long as it is correct for any function $\theta_r(x)$ defining the positions of the credible regions.

Theorem 3. Suppose the expected coverage probability of \hat{p} is equal to $1 - \alpha$ for a positionable credible region generator \mathcal{P}_{θ_r} for all α , x , and $\theta_r(\cdot)$ assigning a position to the credible regions as a function of x . Further suppose that $\hat{p}(\cdot|x)$ and $p(\theta, x)$ are nonzero for all θ and x . Then $\hat{p}(\cdot|x) = p(\cdot|x)$.

Proof Again, let $\Theta := \mathcal{P}_{\theta_r}(\hat{p}, \alpha, x)$ for clarity.

First, we leverage the definition of credible regions to find an expression for the volume of Θ :

$$1 - \alpha = \int_{\Theta} d\theta \hat{p}(\theta|x) = \text{vol}[\Theta] \overline{\hat{p}(\cdot|x)}(\Theta), \quad (9)$$

which implies

$$\text{vol}[\Theta] = \frac{1 - \alpha}{\overline{\hat{p}(\cdot|x)}(\Theta)}. \quad (10)$$

This allows us to expand and simplify the expression for the expected coverage:

$$\begin{aligned} \text{ECP}(\hat{p}, \alpha, \mathcal{P}_{\theta_r}) &= 1 - \alpha \\ &= \int dx p(x) \int_{\Theta} d\theta \hat{p}(\theta|x) \\ &= \int dx p(x) \text{vol}[\Theta] \overline{\hat{p}(\cdot|x)}(\Theta) \\ &= (1 - \alpha) \int dx p(x) \frac{\overline{\hat{p}(\cdot|x)}(\Theta)}{\overline{\hat{p}(\cdot|x)}(\Theta)}. \end{aligned} \quad (11)$$

Canceling the factors of $1 - \alpha$ gives that the integral in the last line is equal to 1.

By assumption, this holds for *any* choice of position function $\theta_r(x)$. We can therefore take the functional derivative of the integral with respect to $\theta_r(x)$. Recalling that the averages in the integrand depend on θ_r , we obtain

$$0 = \frac{\delta}{\delta \theta_r(x)} \int dx p(x) \frac{\overline{\hat{p}(\cdot|x)}(\Theta)}{\overline{\hat{p}(\cdot|x)}(\Theta)} \quad (12)$$

$$= \int dx \delta \theta_{r,i}(x) p(x) \frac{\partial}{\partial \theta_{r,i}} \left(\frac{\overline{\hat{p}(\cdot|x)}(\Theta)}{\overline{\hat{p}(\cdot|x)}(\Theta)} \right) \quad (13)$$

$$\begin{aligned} &= \int dx \delta \theta_{r,i}(x) \frac{\overline{\hat{p}(\cdot|x)}(\Theta) p(x)}{\overline{\hat{p}(\cdot|x)}(\Theta)} \\ &\quad \times \left[\frac{\partial \log \overline{\hat{p}(\cdot|x)}(\Theta)}{\partial \theta_{r,i}} - \frac{\partial \log \overline{p(\cdot|x)}(\Theta)}{\partial \theta_{r,i}} \right], \end{aligned} \quad (14)$$

where the i subscript indexes the components of θ_r . Since this expression must hold for all variations $\delta \theta_{r,i}$, the integrand must evaluate to zero (i.e., the Euler-Lagrange equation must be satisfied). By assumption, the factor outside the braces in the integrand is nonzero, implying

$$\frac{\partial \log \overline{\hat{p}(\cdot|x)}(\Theta)}{\partial \theta_{r,i}} = \frac{\partial \log \overline{p(\cdot|x)}(\Theta)}{\partial \theta_{r,i}}. \quad (15)$$

This implies $\log \overline{p(\cdot|x)}(\Theta) = \log \overline{\hat{p}(\cdot|x)}(\Theta) + c(x)$, for some x -dependent integration constant c . But since the functions inside the logarithms themselves densities, we have $c(\cdot) = 0$. Taking the limit $\alpha \rightarrow 1$ gives $\hat{p}(\theta|x) = p(\theta|x)$. \blacksquare

The coverage testing method we will introduce in the next section is effectively a practical implementation of this theorem.

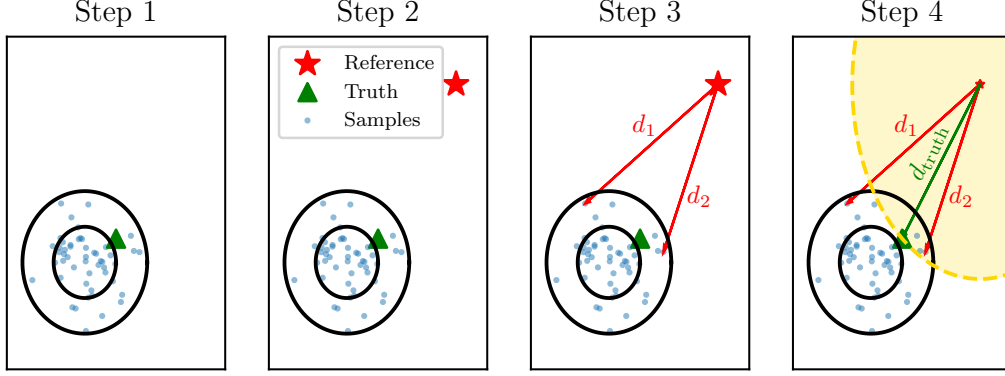


Figure 1. A graphical illustration of our proposed method for coverage probabilities. *Top left*: we use each simulation from the validation set to generate a number of samples n from the posterior estimator. *Top right*: We pick a random location in parameter space as our reference θ_r . *Bottom left*: We calculate the distance d_i between each sample and θ_r . *Bottom right*: We calculate the distance d_{true} between the true value of the parameters θ_{true} , and θ_r (bottom right panel).

3. Our method

With our main theoretical result proven (c.f. Theorem 3), in this section we use it to first explain the blind spots of typical coverage probability calculations and then introduce our new coverage checking procedure.

3.1. High posterior density coverage testing

Before introducing our method, we first discuss HPD coverage.

HPD credible regions are often used to assess coverage (Hermans et al., 2021b; Rozet et al., 2021; Miller et al., 2022a; Deistler et al., 2022; Tejero-Cantero et al., 2020). Perhaps the most intuitive way of calculating expected coverage probability using HPD regions is to compute such a region for every value of α , then calculate the expected coverage using (3). In practice, however, there is a more efficient calculation of expected coverage probabilities, which is derived from the following:

Definition 5. A pair (θ^*, x^*) , and a posterior estimator $\hat{p}(\theta|x)$ uniquely define a HPD confidence region as:

$$\Theta_{\text{HPD}}(x^*, \theta^*, \hat{p}) := \{\theta \in U \mid \hat{p}(\theta|x^*) \geq \hat{p}(\theta^*|x^*)\}. \quad (16)$$

This, in turn, defines a corresponding **HPD confidence level** $1 - \tilde{\alpha}_{\text{HPD}}(\hat{p}, \theta^*, x^*)$. We denote the generator of HPD credible regions as \mathcal{H} .

We can then rederive an important result for this HPD confidence level:

Lemma 1. We can calculate the ECP of the $1 - \alpha$ highest

posterior density regions as:

$$\text{ECP}(\hat{p}, \alpha) = \mathbb{E}_{p(\theta, x)} [\mathbb{1}(\tilde{\alpha}_{\text{HPD}}(\hat{p}, \theta, x) \geq \alpha)]. \quad (17)$$

Proof Firstly, we notice that:

$$\theta^* \in \Theta_{\text{HPD}}(x^*, \alpha, \hat{p}) \Leftrightarrow \tilde{\alpha}_{\text{HPD}}(\hat{p}, \theta^*, x^*) \geq \alpha. \quad (18)$$

This follows from the fact that, if $\theta^* \in \Theta_{\text{HPD}}(x^*, \alpha, \hat{p})$, then the HPD confidence region defined by (θ^*, x^*) is contained in $\Theta_{\text{HPD}}(x^*, \alpha, \hat{p})$.

Then, from (4), it follows that (17) is true. \blacksquare

This result can be used in practice to calculate the HPD ECP from samples of the true joint distribution $p(\theta, x)$, as shown in Algorithm 1. As previously discussed, this algorithm requires explicit evaluations of the posterior estimator. We try to provide more intuitive connections between both definitions in §A.

As is well-known in the literature, estimating the ECP with HPD regions is not enough to demonstrate a posterior estimator is optimal. Theorem 3 reveals why: by definition, the HPD region generator is not positionable. Positionability is critical to the proof of the theorem, since it requires varying the position function $\theta_r(x)$.

To concretely demonstrate how considering only HPD coverage can fail, we consider the interesting case discussed in

Algorithm 1 Calculation of ECP(\hat{p}, α) using highest posterior density regions, from a set of simulations $\{\theta_i, x_i\}$, $i \in [1, N_{\text{sims}}]$

Generate n samples $\{\theta_{ij}\} \sim \hat{p}(\theta|x_i)$ for each simulation x_i .

for $i \leftarrow 1$ to N_{sims} **do**

$$f_i = (1/n) \cdot \sum_{j=1}^n \mathbb{1}[\hat{p}(\theta_{ij}|x_i) < \hat{p}(\theta_i^*|x_i)]$$

end for

$$\text{ECP}(\hat{p}, \alpha) = (1/N_{\text{sims}}) \sum_{i=1}^{N_{\text{sims}}} \mathbb{1}(f_i < 1 - \alpha)$$

H21 of $\hat{p}(\theta|x) = p(\theta)$. From the definition of ECP,

$$\begin{aligned} \text{ECP}(\hat{p}, \alpha, \mathcal{H}) &= \mathbb{E}_{p(x, \theta)}[\mathbb{1}(\theta \in \mathcal{H}(\hat{p}, \alpha))] \\ &= \mathbb{E}_{p(\theta)}[\mathbb{1}(\theta \in \mathcal{H}(\hat{p}, \alpha))] \\ &= \int_{\mathcal{H}(\hat{p}, \alpha)} d\theta p(\theta) \\ &= 1 - \alpha. \end{aligned} \quad (19)$$

In the second line, we used the fact that HPD generator is independent of x in this case. We recognize the third line as the definition of a credible region for the prior, yielding the fourth line. This means that $\hat{p}(\theta|x)$ has perfect HPD ECP in this case.

We now introduce a coverage testing method that remedies such blind spots.

3.2. Distance to random point coverage testing

Our method generates spherical credible regions around position θ_r :

Definition 6. A pair (θ^*, x^*) , and a posterior estimator $\hat{p}(\theta|x)$ uniquely define a **distance to random point (DRP) credible region** for a given d and θ_r :

$$\Theta_{\text{DRP}}(x^*, \theta^*, \hat{p}, \theta_r) = \{\theta \in U \mid d(\theta, \theta_r) \leq d(\theta^*, \theta_r)\} \quad (20)$$

This, in turn, defines a corresponding **DRP confidence level** $1 - \tilde{\alpha}_{\text{DRP}}(\hat{p}, \theta^*, \theta_r, d)$. We call the generator of DRP regions \mathcal{D}_{θ_r} .

We can calculate expected coverage similarly to the HPD case:

Lemma 2. We can calculate the ECP of the $1 - \alpha$ highest posterior density regions as:

$$\text{ECP}(\hat{p}, \alpha) = \mathbb{E}_{p(\theta, x)}[\mathbb{1}(\tilde{\alpha}_{\text{DRP}}(\hat{p}, \theta^*, \theta_r, x^*, d) \geq \alpha)]. \quad (21)$$

Proof Let $\mathcal{D}_{\theta_r}(x^*, \alpha, \hat{p})$ be a ball centered at θ_r with radius $R(\alpha)$ and credibility $1 - \alpha$. Similarly, the DRP region defined by (θ^*, x^*) has the same center, radius $d(\theta^*, \theta_r)$, and credibility $1 - \tilde{\alpha}$ for some $\tilde{\alpha}$. It then follows that:

$$\theta^* \in \mathcal{D}_{\theta_r}(x^*, \alpha, \hat{p}) \Leftrightarrow d(\theta^*, \theta_r) \leq R(\alpha). \quad (22)$$

Since R is a monotonic function of α and the regions are centered on the same point, we have

$$d(\theta^*, \theta_r) < R(\alpha) \Leftrightarrow \tilde{\alpha} \geq \alpha. \quad (23)$$

Then by (4) we have (21). \blacksquare

With this, we have everything we need to formulate our algorithm, which is presented in Algorithm 2. While similar to Algorithm 1, there are two key differences to this algorithm:

- DRP implements Theorem 3's requirement that coverage holds for all possible ways of choosing the positions of the credible regions by randomly sampling θ_r from some distribution $\tilde{p}(\theta|x)$ that can depend on x .
- DRP probes credible regions of smaller size (i.e., larger α) as the number of posterior samples, simulations and reference points tested is increased. Following the login of the proof of Theorem 3, this means it asymptotically tests whether the averages of $\hat{p}(\theta|x)$ and $p(\theta|x)$ match on smaller and small balls.
- DRP does not require explicit evaluations of the posterior estimator \hat{p} : it only requires calculating distances between parameters sampled from \hat{p} and θ_r .

In the following section, we test our method in a series of experiments and compare its performance with that of HPD coverage probabilities.

4. Experiments

We apply our algorithm, described in Algorithm 2 to three different experiments. For all experiments, we normalize all parameters θ to the range $[0, 1]$, and unless otherwise specified, we generate reference points uniformly in the D -dimensional hypercube $x \in [0, 1]^D$ where D is the dimensionality of the parameter space. We use the Euclidean or L2 distance as a metric to calculate DRP regions.

4.1. Gaussian Toy Model

As a first example, we can use a simple Gaussian toy model. In this model, we assume that all the posterior distributions

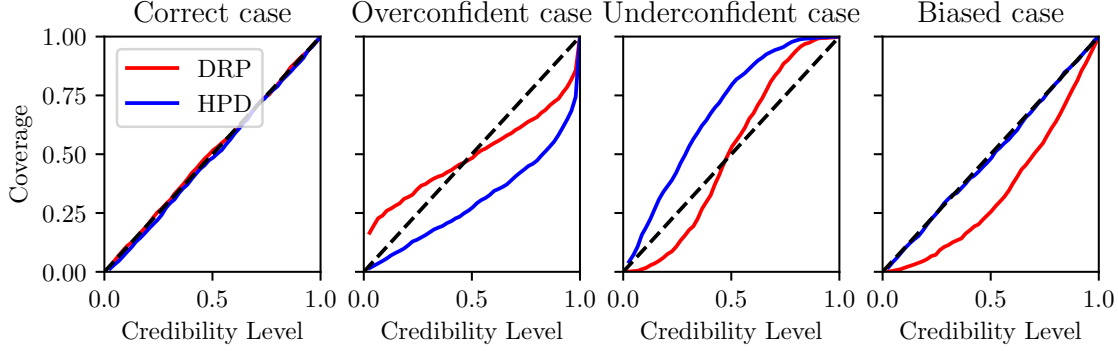


Figure 2. Results on the Gaussian toy model for all four cases described in §4.1. The red line shows the method presented in this paper, while the blue shows the HPD region.

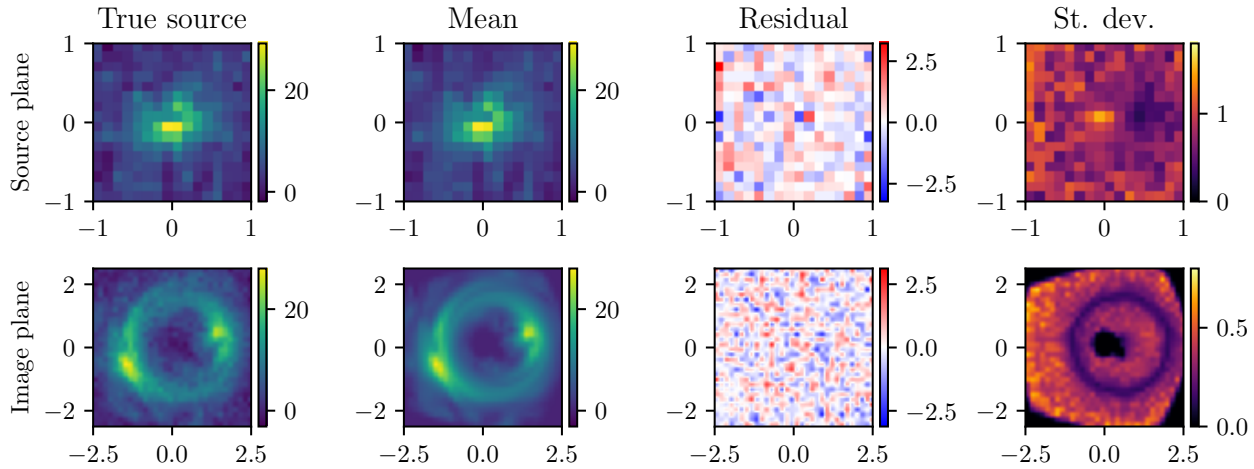


Figure 3. An example of one of our lensing simulations. The top panels show the source plane that we are trying to infer, while the bottom panels show the distorted light. From left to right, the plot shows truth, mean and standard deviation of the samples from our posterior estimator (in the case of this figure, the ‘exact’ estimator), and the residuals. The noise in the observations is set to 1 on the color scales shown here.

are Gaussian. Therefore, we can generate samples from the posterior for a validation simulation from the estimated mean and covariance matrix. We first generate ‘simulations’, by uniformly sampling in our parameter space:

$$\theta_{\text{true}} \sim \mathcal{U}(-5, 5). \quad (24)$$

We also randomly generate the diagonal elements of the covariances matrices Σ of our posterior estimates (assumed to have no non-diagonal elements).

$$\log \sigma \sim \mathcal{U}(-5, -1), \quad (25)$$

To validate, we also need to know the mean of the posterior distributions. We consider three cases:

- Firstly, we draw these from a normal distribution $\mathcal{N}(\theta_{\text{true}}, \Sigma)$. This means that the coverage probabili-

ties should show a uniform distribution. We call this the *correct case*.

- Secondly, we draw the true values from $\mathcal{N}(\theta_{\text{true}}, 0.5\Sigma)$ and $(\mathcal{N}(\theta_{\text{true}}, 2\Sigma))$. This means that the posterior samples come from a distribution that is too narrow (wide), and are therefore overconfident (underconfident)
- Lastly, we want to build a *biased case*. For this, we pick the means to be equal to:

$$\theta_{\text{true}} - \text{sign}(\theta_{\text{true}}) \cdot Z \left(1 - \frac{|\theta_{\text{true}}|}{5} \right) \cdot \sigma, \quad (26)$$

where Z is the inverse survival function. The idea with this example is to create a position-dependent bias: The furthest the true value is from the origin, the more biased the posterior is. We have specifically designed

Algorithm 2 Calculation of $ECP(\hat{p}, \alpha)$ using the DRP method, using a set of simulations $\{\theta_i, x_i\}$, $i \in \{1, \dots, N_{\text{sims}}\}$, parameter distance metric $d : U \times U \rightarrow \mathbb{R}$ and reference point sampling distribution $\tilde{p}(\cdot|x)$.

```

Generate  $n$  samples  $\{\theta_{ij}\} \sim \hat{p}(\theta|x_i)$  for each simulation  $x_i$ , where  $j = \{1, \dots, n\}$ .
for  $i \leftarrow 1$  to  $N_{\text{sims}}$  do
     $\theta_r \sim \tilde{p}(\theta_r|x)$  {Generate reference point}
     $f_i = (1/n) \cdot \sum_{j=1}^n \mathbb{1}[d(\theta_{ij}, \theta_r) < d(\theta_i^*, \theta_r)]$ 
end for
 $ECP(\hat{p}, \alpha) = (1/N_{\text{sims}}) \sum_{i=1}^{N_{\text{sims}}} \mathbb{1}(f_i < 1 - \alpha)$ 

```

this bias in a way that HPC coverage probabilities will be blind to it. However, the point of this example is to show that there are biases that HPC can be blind to, but the random nature of DRP should be able to detect.

For each of these cases, we want to compare how our method compares to the HPD coverage probability test. Because in this toy model we know the correct posterior, we can easily compute both HPD and DRP coverage probabilities. To pick the DRP reference points, we use the prior ($\tilde{p}(\theta_r|x) = p(\theta_r)$).

The results for our Gaussian toy model are shown in Fig. 2. In each panel, the x -axis shows the credibility level $1 - \alpha$, while the y -axis shows the expected coverage $ECP(\hat{p}, \alpha)$. For an optimal posterior estimator, $ECP(\hat{p}, \alpha) = 1 - \alpha$, $\forall \alpha \in (0, 1)$ as described in § 2, which would then lead to the diagonal black dashed diagonal line. We see in the first panel that that is indeed the case for the ‘correct’ case, which is optimal by construction. We found consistent results amongst all values of D we tested, going up to $D = 1000$.

The second and third panels show the over and underconfident cases, respectively. We see how these cases lead to different coverage plots than the HPD method. This is not entirely unexpected: For underconfident estimators, the DRP regions from randomly selected points are more likely to cover approximately half of the posterior estimator $\alpha \sim 0.5$, while for overconfident estimators, they are likely to cover either very little $\alpha \sim 1$ or a lot $\alpha \sim 0$. We expand this intuition, including some figures, in § B. Finally, in the fourth panel, we see how the biased case cannot be detected by the HPD region but is detectable by DRP. This shows how, as explained in § 2, $ECP(\hat{p}, \alpha) = 1 - \alpha$ does not mean the posterior is optimal for HPD regions, but it does for DRP regions.

4.2. Revealing when estimators are uninformative

As our second benchmark, we consider the case mentioned before in which the learned posterior estimator is equal to the prior $\hat{p}(\theta|x) = p(\theta)$. The reason why we are interested in this example is that, in that case, the expected coverage probability calculated using HPD regions will be equal to

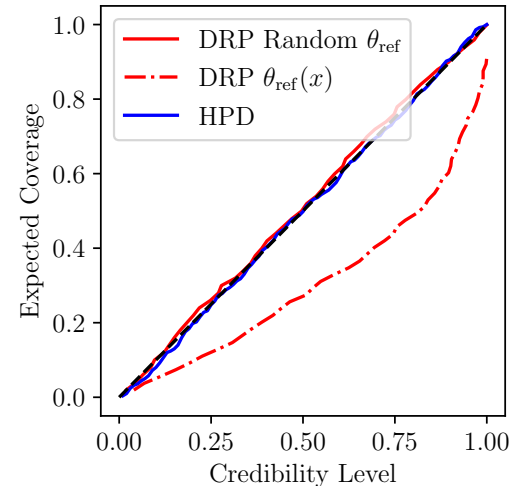


Figure 4. Expected coverage vs probability level for the uninformative posterior estimator described in § 4.2. The blue line shows the coverage calculated using HPD regions, while the red lines use DRP regions. The continuous line uses reference points that are independent of x , while the dot-dashed line uses reference points that depend on x .

$1 - \alpha$ for any value of α , as previously discussed. However, with DRP we have the ability to avoid this blindspot by sampling reference points in a manner dependent on x .

To make this concrete, we consider a one-dimensional example with a Gaussian prior $p(\theta) = \mathcal{N}(\theta; \mu_0, \sigma_0^2)$. Our ‘forward model’ in this case is simply generating a number n_x of data points, from $\{x_i\}_{i=1}^{n_x} \sim N(\theta, \sigma^2)$. In this conjugate model, we can easily derive the true posterior:

$$p(\theta | \{x_i\}_{i=1}^{n_x}) = \mathcal{N}(\mu | m, s), \quad (27)$$

$$s = \left(\frac{1}{\sigma_0^2} + \frac{n+x}{\sigma^2} \right)^{-1}, \quad (28)$$

$$m = s \left(\frac{\mu_0}{\sigma_0^2} + \frac{\sum_i x_i}{\sigma^2} \right) \quad (29)$$

We fix $n_x = 50$, $\mu_0 = 0$, $\sigma_0 = 1$ and $\sigma_x = 0.1$. We generate 500 samples from the forward model, and calculate expected coverage from an ‘uninformative estimator’

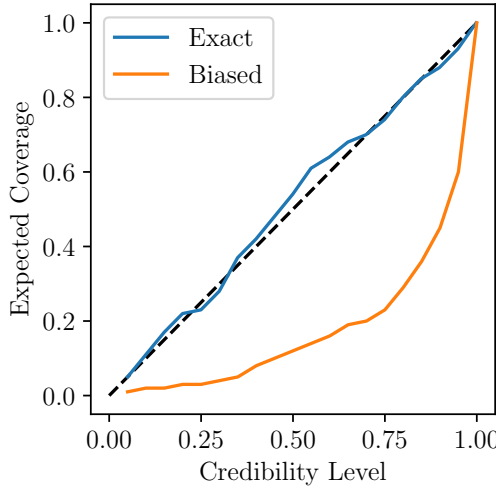


Figure 5. Coverage probability vs credibility level for our lensing example. We see how, as expected, the exact estimator (blue) produces optimal posteriors.

$\hat{p}(\theta|x) = p(\theta)$ in three ways: 1) using HPD regions, 2) using DRP regions where θ_r is drawn randomly from the prior, and 3) using DRP regions where $\theta_r = x_0 + u$, where x_0 is the first observation, and $u \sim \mathcal{U}(-1, 1)$. We expect the first two methods to have ECP equal to $1 - \alpha$, but for the third to not.

We show the results in Fig. 4. First, we notice that when we use HPD regions, we get the correct expected coverage, even though the estimator is wrong (validating the theoretical discussion in § 2). This means that, in this case, HPD coverage could fool us into thinking our estimator is optimal when in reality it is completely uninformative. Interestingly, the same happens when we use DRP regions with reference points selected randomly from the prior (red line). This is because, as discussed in § 2, Theorem 3 only holds in both directions when the choice of the region depends on x . Finally, as anticipated, the expected coverage is *not* $1 - \alpha$ when the sampling distribution for θ_r has some x -dependence. Therefore, we see how even when we introduce a small dependence on x to $\tilde{p}(\theta_r|x)$ in DRP reveals that the posterior estimator is not optimal.

4.3. Gravitational Lensing

To test our algorithm in a more realistic and high-dimensional setting, we consider a simplified astrophysics problem: gravitational lensing source reconstruction. Gravitational lensing occurs in nature when light rays from a distant galaxy move along curved rather than straight paths due to the mass of another intervening galaxy (the ‘lens’) (Treu, 2010). The result is a highly-distorted, ring-shaped

image of the background galaxy. The goal of source reconstruction is to infer from a noisy image what the light from the source galaxy looks like without distortions, assuming the mathematical form of the distortions is perfectly known.

The simulator in this scenario samples the source galaxy’s light θ from a multivariate-normal distribution that we fit to a dataset of galaxy images (Stone & Courteau, 2019; Stone et al., 2021). A matrix A encoding the lensing distortions are then applied, and the final observation is produced by adding Gaussian pixel noise of standard deviation σ_n , so that $x \sim \mathcal{N}(A\theta, \sigma_n^2)$. For computational convenience, we use 16×16 -pixel source images and 32×32 -pixel observations.

As shown in Adam et al. (2022) and reviewed in §C, posterior samples of θ can be generated using techniques from diffusion modeling. In general, this approach yields subtly biased posterior samples. However, with our multivariate-normal prior on θ , it is possible to generate unbiased posterior samples. We refer to samples from these as ‘biased’ and ‘exact’ in our results.

Fig. 5 shows the results for both the exact and the biased posterior estimators, using 100 simulations, and 1000 posterior samples per simulation, and sampling θ_r from the prior. As expected, our method gets the correct coverage for the exact estimator. It is important to stress that generative models are needed for parameter spaces of this dimensionality (256 parameters), and no previously existing methods could calculate ECPs to assess the optimality of such models. The biased estimator, on the other hand, produces a similar curve to that of the bottom right panel of Fig. 2, which indicates that it is indeed biased.

5. Conclusions

Testing the accuracy of estimated posteriors is a key element of parameter inference. While there exist well-established methods to test posterior sampling techniques such as MCMC, it is difficult to test the accuracy of posterior estimated from alternative methods such as deep learning methods. This is the case for both likelihood-based and simulation-based inference. In this paper, we introduced DRP coverage probabilities as a new technique to test the accuracy of estimated posteriors using posterior samples alone, when explicit posterior evaluations are not available. We have shown that this test is sufficient to prove that the inference is optimal, while other similar tests were necessary but not sufficient.

We applied our test successfully to a variety of inference problems, in particular in cases where alternative methods fail, and shown that it scales well to high-dimensional posteriors. Therefore, we propose DRP coverage probabilities as a tool to test the accuracy of future posterior inference analyses from generative models.

Acknowledgements

We would like to thank Bruno Regaldo, Shirley Ho and Nikolay Malkin for their feedback on preliminary versions of the paper.

This research was made possible by a generous donation by Eric and Wendy Schmidt with the recommendation of the Schmidt Futures Foundation. The work is in part supported by computational resources provided by Calcul Québec and the Digital Research Alliance of Canada. Y.H. and L.P. acknowledge support from the National Sciences and Engineering Council of Canada grant RGPIN-2020-05102, the Fonds de recherche du Québec grant 2022-NC-301305 and 300397, and the Canada Research Chairs Program. P.L acknowledges support from the Simons Foundation.

References

Adam, A., Coogan, A., Malkin, N., Legin, R., Perreault-Levasseur, L., Hezaveh, Y., and Bengio, Y. Posterior samples of source galaxies in strong gravitational lenses with score-based priors. *arXiv preprint arXiv:2211.03812*, 2022.

Alsing, J., Charnock, T., Feeney, S., and Wandelt, B. Fast likelihood-free cosmology with neural density estimators and active learning. *Monthly Notices of the Royal Astronomical Society*, 488(3):4440–4458, 2019.

Anau Montel, N. and Weniger, C. Detection is truncation: studying source populations with truncated marginal neural ratio estimation. In *36th Conference on Neural Information Processing Systems*, 11 2022.

Beaumont, M. A., Zhang, W., and Balding, D. J. Approximate bayesian computation in population genetics. *Genetics*, 162(4):2025–2035, 2002.

Brehmer, J. Simulation-based inference in particle physics. *Nature Reviews Physics*, 3(5):305–305, January 2021. doi: 10.1038/s42254-021-00305-6.

Brehmer, J., Mishra-Sharma, S., Hermans, J., Louppe, G., and Cranmer, K. Mining for Dark Matter Substructure: Inferring subhalo population properties from strong lenses with machine learning. *Astrophys. J.*, 886(1):49, 2019. doi: 10.3847/1538-4357/ab4c41.

Charnock, T., Perreault-Levasseur, L., and Lanusse, F. Bayesian Neural Networks. *arXiv e-prints*, art. arXiv:2006.01490, June 2020. doi: 10.48550/arXiv.2006.01490.

Coogan, A., Karchev, K., and Weniger, C. Targeted Likelihood-Free Inference of Dark Matter Substructure in Strongly-Lensed Galaxies. In *34th Conference on Neural Information Processing Systems*, 10 2020.

Coogan, A., Anau Montel, N., Karchev, K., Grootes, M. W., Nattino, F., and Weniger, C. One never walks alone: the effect of the perturber population on subhalo measurements in strong gravitational lenses. 9 2022.

Cranmer, K., Pavez, J., and Louppe, G. Approximating likelihood ratios with calibrated discriminative classifiers. *arXiv preprint arXiv:1506.02169*, 2015.

Cranmer, K., Brehmer, J., and Louppe, G. The frontier of simulation-based inference. *Proceedings of the National Academy of Sciences*, 117(48):30055–30062, 2020.

Dalmasso, N., Pospisil, T., Lee, A. B., Izbicki, R., Freeman, P. E., and Malz, A. I. Conditional density estimation tools in python and r with applications to photometric redshifts and likelihood-free cosmological inference. *Astronomy and Computing*, 30:100362, 2020.

Dax, M., Green, S. R., Gair, J., Macke, J. H., Buonanno, A., and Schölkopf, B. Real-time gravitational wave science with neural posterior estimation. *Phys. Rev. Lett.*, 127:241103, Dec 2021. doi: 10.1103/PhysRevLett.127.241103. URL <https://link.aps.org/doi/10.1103/PhysRevLett.127.241103>.

de Witt, C. S., Gram-Hansen, B., Nardelli, N., Gambardella, A., Zinkov, R., Dokania, P., Siddharth, N., Espinosa-Gonzalez, A. B., Darzi, A., Torr, P., and Baydin, A. G. Simulation-based inference for global health decisions. 2020. doi: 10.48550/ARXIV.2005.07062. URL <https://arxiv.org/abs/2005.07062>.

Deistler, M., Goncalves, P. J., and Macke, J. H. Truncated proposals for scalable and hassle-free simulation-based inference. *arXiv preprint arXiv:2210.04815*, 2022.

Dinh, L., Krueger, D., and Bengio, Y. Nice: Non-linear independent components estimation. *arXiv preprint arXiv:1410.8516*, 2014.

Durkan, C., Murray, I., and Papamakarios, G. On contrastive learning for likelihood-free inference. In *International Conference on Machine Learning*, pp. 2771–2781. PMLR, 2020.

Fearnhead, P. and Prangle, D. Constructing summary statistics for approximate bayesian computation: semi-automatic approximate bayesian computation. *Journal of the Royal Statistical Society: Series B (Statistical Methodology)*, 74(3):419–474, 2012.

Frazier, D. T., Nott, D. J., Drovandi, C., and Kohn, R. Bayesian inference using synthetic likelihood: asymptotics and adjustments. *Journal of the American Statistical Association*, (just-accepted):1–28, 2022.

Gelman, A. and Rubin, D. B. Inference from iterative simulation using multiple sequences. *Statistical science*, pp. 457–472, 1992.

Gonçalves, P. J., Lueckmann, J.-M., Deistler, M., Nonnenmacher, M., Öcal, K., Bassetto, G., Chintaluri, C., Podlaski, W. F., Haddad, S. A., Vogels, T. P., Greenberg, D. S., and Macke, J. H. Training deep neural density estimators to identify mechanistic models of neural dynamics. *eLife*, 9:e56261, sep 2020. ISSN 2050-084X. doi: 10.7554/eLife.56261. URL <https://doi.org/10.7554/eLife.56261>.

Goodfellow, I. J., Pouget-Abadie, J., Mirza, M., Xu, B., Warde-Farley, D., Ozair, S., Courville, A., and Bengio, Y. Generative adversarial nets. *stat*, 1050:10, 2014.

Greenberg, D., Nonnenmacher, M., and Macke, J. Automatic posterior transformation for likelihood-free inference. In *International Conference on Machine Learning*, pp. 2404–2414. PMLR, 2019.

Guo, C., Pleiss, G., Sun, Y., and Weinberger, K. Q. On Calibration of Modern Neural Networks. *arXiv e-prints*, art. arXiv:1706.04599, June 2017. doi: 10.48550/arXiv.1706.04599.

Hermans, J., Begy, V., and Louppe, G. Likelihood-free mcmc with amortized approximate ratio estimators. In *International Conference on Machine Learning*, pp. 4239–4248. PMLR, 2020.

Hermans, J., Banik, N., Weniger, C., Bertone, G., and Louppe, G. Towards constraining warm dark matter with stellar streams through neural simulation-based inference. *Mon. Not. Roy. Astron. Soc.*, 507(2):1999–2011, 2021a. doi: 10.1093/mnras/stab2181.

Hermans, J., Delaunoy, A., Rozet, F., Wehenkel, A., and Louppe, G. Averting a crisis in simulation-based inference. *arXiv preprint arXiv:2110.06581*, 2021b.

Ho, J., Jain, A., and Abbeel, P. Denoising diffusion probabilistic models. *CoRR*, abs/2006.11239, 2020. URL <https://arxiv.org/abs/2006.11239>.

Hyvärinen, A. and Dayan, P. Estimation of non-normalized statistical models by score matching. *Journal of Machine Learning Research*, 6(4), 2005.

Karchev, K., Anau Montel, N., Coogan, A., and Weniger, C. Strong-Lensing Source Reconstruction with Denoising Diffusion Restoration Models. In *36th Conference on Neural Information Processing Systems*, 11 2022a.

Karchev, K., Trotta, R., and Weniger, C. SICRET: Supernova Ia Cosmology with truncated marginal neural Ratio EsTimation. 9 2022b. doi: 10.1093/mnras/stac3785.

Kingma, D. P. and Welling, M. Auto-encoding variational bayes. *arXiv preprint arXiv:1312.6114*, 2013.

Legin, R., Hezaveh, Y., Levasseur, L. P., and Wandelt, B. Simulation-Based Inference of Strong Gravitational Lensing Parameters. 12 2021.

Linhart, J., Gramfort, A., and Rodrigues, P. L. Validation diagnostics for sbi algorithms based on normalizing flows. *arXiv preprint arXiv:2211.09602*, 2022.

Lueckmann, J.-M., Goncalves, P. J., Bassetto, G., Öcal, K., Nonnenmacher, M., and Macke, J. H. Flexible statistical inference for mechanistic models of neural dynamics. *Advances in neural information processing systems*, 30, 2017.

Lueckmann, J.-M., Bassetto, G., Karaletsos, T., and Macke, J. H. Likelihood-free inference with emulator networks. *arXiv e-prints*, art. arXiv:1805.09294, May 2018.

Lueckmann, J.-M., Boelts, J., Greenberg, D., Goncalves, P., and Macke, J. Benchmarking simulation-based inference. In *International Conference on Artificial Intelligence and Statistics*, pp. 343–351. PMLR, 2021.

Marjoram, P., Molitor, J., Plagnol, V., and Tavaré, S. Markov chain monte carlo without likelihoods. *Proceedings of the National Academy of Sciences*, 100(26):15324–15328, 2003.

Marlier, N., Brüls, O., and Louppe, G. Simulation-based bayesian inference for multi-fingered robotic grasping, 2021. URL <https://arxiv.org/abs/2109.14275>.

Miller, B. K., Cole, A., Weniger, C., Nattino, F., Ku, O., and Grootes, M. W. swyft: Truncated marginal neural ratio estimation in python. *Journal of Open Source Software*, 7(75):4205, 2022a. doi: 10.21105/joss.04205. URL <https://doi.org/10.21105/joss.04205>.

Miller, B. K., Weniger, C., and Forré, P. Contrastive Neural Ratio Estimation. 10 2022b.

Mishra-Sharma, S. and Cranmer, K. Neural simulation-based inference approach for characterizing the Galactic Center γ -ray excess. *Phys. Rev. D*, 105(6):063017, 2022. doi: 10.1103/PhysRevD.105.063017.

Montel, N. A., Coogan, A., Correa, C., Karchev, K., and Weniger, C. Estimating the warm dark matter mass from strong lensing images with truncated marginal neural ratio estimation. *Mon. Not. Roy. Astron. Soc.*, 518(2):2746–2760, 2022. doi: 10.1093/mnras/stac3215.

Ong, V. M.-H., Nott, D. J., Tran, M.-N., Sisson, S. A., and Drovandi, C. C. Likelihood-free inference in high

dimensions with synthetic likelihood. *Computational Statistics & Data Analysis*, 128:271–291, 2018.

Papamakarios, G. and Murray, I. Fast ε -free inference of simulation models with bayesian conditional density estimation. *Advances in neural information processing systems*, 29, 2016.

Papamakarios, G., Sterratt, D., and Murray, I. Sequential neural likelihood: Fast likelihood-free inference with autoregressive flows. In *The 22nd International Conference on Artificial Intelligence and Statistics*, pp. 837–848. PMLR, 2019.

Papamakarios, G., Nalisnick, E. T., Rezende, D. J., Mohamed, S., and Lakshminarayanan, B. Normalizing flows for probabilistic modeling and inference. *J. Mach. Learn. Res.*, 22(57):1–64, 2021.

Papernot, N. and McDaniel, P. Deep k-Nearest Neighbors: Towards Confident, Interpretable and Robust Deep Learning. *arXiv e-prints*, art. arXiv:1803.04765, March 2018. doi: 10.48550/arXiv.1803.04765.

Perreault Levasseur, L., Hezaveh, Y. D., and Wechsler, R. H. Uncertainties in Parameters Estimated with Neural Networks: Application to Strong Gravitational Lensing. *Astrophys. J. Lett.*, 850(1):L7, 2017. doi: 10.3847/2041-8213/aa9704.

Prangle, D., Blum, M., Popovic, G., and Sisson, S. Diagnostic tools of approximate bayesian computation using the coverage property.” *arxiv preprint. arXiv preprint arXiv:1301.3166*, 412, 2013.

Price, L. F., Drovandi, C. C., Lee, A., and Nott, D. J. Bayesian synthetic likelihood. *Journal of Computational and Graphical Statistics*, 27(1):1–11, 2018.

Pritchard, J. K., Seielstad, M. T., Perez-Lezaun, A., and Feldman, M. W. Population growth of human y chromosomes: a study of y chromosome microsatellites. *Molecular biology and evolution*, 16(12):1791–1798, 1999.

Ramesh, P., Lueckmann, J.-M., Boelts, J., Tejero-Cantero, Á., Greenberg, D. S., Gonçalves, P. J., and Macke, J. H. GATSBI: Generative Adversarial Training for Simulation-Based Inference. *arXiv e-prints*, art. arXiv:2203.06481, March 2022. doi: 10.48550/arXiv.2203.06481.

Rezende, D. and Mohamed, S. Variational inference with normalizing flows. In *International conference on machine learning*, pp. 1530–1538. PMLR, 2015.

Rozet, F. et al. Arbitrary marginal neural ratio estimation for likelihood-free inference. 2021.

Rubin, D. B. Bayesianly Justifiable and Relevant Frequency Calculations for the Applied Statistician. *The Annals of Statistics*, 12(4):1151 – 1172, 1984. doi: 10.1214/aos/1176346785. URL <https://doi.org/10.1214/aos/1176346785>.

Schall, R. The empirical coverage of confidence intervals: Point estimates and confidence intervals for confidence levels. *Biometrical journal*, 54(4):537–551, 2012.

Sohl-Dickstein, J., Weiss, E. A., Maheswaranathan, N., and Ganguli, S. Deep unsupervised learning using nonequilibrium thermodynamics. *CoRR*, abs/1503.03585, 2015. URL <http://arxiv.org/abs/1503.03585>.

Song, Y., Sohl-Dickstein, J., Kingma, D. P., Kumar, A., Ermon, S., and Poole, B. Score-based generative modeling through stochastic differential equations. *arXiv preprint arXiv:2011.13456*, 2020.

Stone, C. and Courteau, S. The Intrinsic Scatter of the Radial Acceleration Relation. *The Astrophysical Journal*, 882(1):6, September 2019. doi: 10.3847/1538-4357/ab3126.

Stone, C., Courteau, S., and Arora, N. The Intrinsic Scatter of Galaxy Scaling Relations. *The Astrophysical Journal*, 912(1):41, May 2021. doi: 10.3847/1538-4357/abebe4.

Talts, S., Betancourt, M., Simpson, D., Vehtari, A., and Gelman, A. Validating bayesian inference algorithms with simulation-based calibration. *arXiv preprint arXiv:1804.06788*, 2018.

Tejero-Cantero, A., Boelts, J., Deistler, M., Lueckmann, J.-M., Durkan, C., Gonçalves, P., Greenberg, D., and Macke, J. sbi: A toolkit for simulation-based inference. *The Journal of Open Source Software*, 5(52):2505, August 2020. doi: 10.21105/joss.02505.

Thomas, O., Dutta, R., Corander, J., Kaski, S., and Gutmann, M. U. Likelihood-free inference by ratio estimation. *Bayesian Analysis*, 17(1):1–31, 2022.

Treu, T. Strong lensing by galaxies. *Annual Review of Astronomy and Astrophysics*, 48:87–125, 2010.

Vincent, P. A connection between score matching and denoising autoencoders. *Neural computation*, 23(7):1661–1674, 2011.

Wagner-Carena, S., Park, J. W., Birrer, S., Marshall, P. J., Roodman, A., and Wechsler, R. H. Hierarchical Inference with Bayesian Neural Networks: An Application to Strong Gravitational Lensing. *Astrophys. J.*, 909(2):187, 2021. doi: 10.3847/1538-4357/abdf59.

Wilson, A. G. and Izmailov, P. Bayesian deep learning and a probabilistic perspective of generalization. In Larochelle,

H., Ranzato, M., Hadsell, R., Balcan, M., and Lin, H. (eds.), *Advances in Neural Information Processing Systems*, volume 33, pp. 4697–4708. Curran Associates, Inc., 2020. URL <https://proceedings.neurips.cc/paper/2020/file/322f62469c5e3c7dc3e58f5a4d1ea399-Paper.pdf>.

Zhu, Y. and Zabaras, N. Bayesian deep convolutional encoder-decoder networks for surrogate modeling and uncertainty quantification. *Journal of Computational Physics*, 366:415–447, August 2018. doi: 10.1016/j.jcp.2018.04.018.

Zuo, Y., Chen, C., Li, X., Deng, Z., Chen, Y., Behler, J., Csányi, G., Shapeev, A. V., Thompson, A. P., Wood, M. A., and Ong, S. P. Performance and cost assessment of machine learning interatomic potentials. *The Journal of Physical Chemistry A*, 124(4):731–745, 2020. doi: 10.1021/acs.jpca.9b08723. URL <https://doi.org/10.1021/acs.jpca.9b08723>. PMID: 31916773.

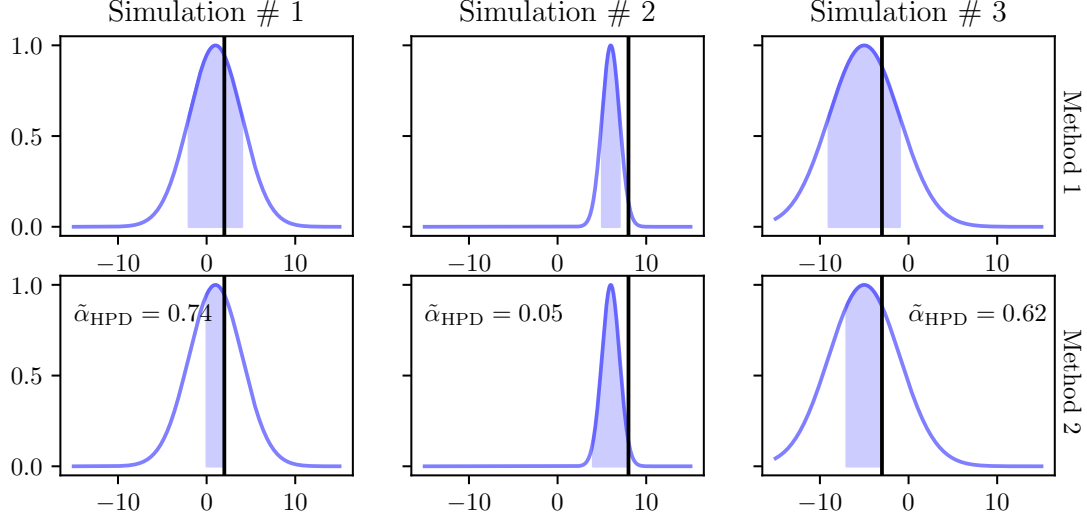


Figure 6. This figure illustrates the intuition behind the two ways of calculating high posterior density coverages. Each column shows one of three simulations in a toy example. The blue curves show the predicted posteriors, and the black vertical lines show the corresponding truths. We want to calculate the coverage for the 68% credibility level ($\alpha = 0.32$). The first approach, shown in the top row, would consist of calculating the $1 - \alpha$ credibility region, then checking how often the truth is in said region (in this case twice, so the coverage is $2/3$). The alternative approach, described in §3.1., and shown in the bottom row, is to find the HPD region defined by the truth, then find how often $\tilde{\alpha}_{\text{HPD}} < \alpha$, which is again twice. The plot illustrates the fact that these two approaches are exactly equivalent.

A. Connection between both definitions

§3.1 discussed the differences between two possible methods for calculating coverage probabilities, both for HPD and DRP regions. We try to build more intuition behind that connection in this appendix. Focusing first on the case of HPD regions, shown in Fig. 6. The first method, perhaps more intuitive but far more inefficient, would be to calculate the $1 - \alpha$ credibility region, then check how often the truth is in said region for each simulation, and for multiple values of alpha (notice the nested loop). The second method, a consequence of the very important Lemma 1, and already used by Algorithm 1 would be to find the HPD region defined by the truth for each simulation, and its corresponding credibility level $1 - \tilde{\alpha}_{\text{HPD}}$. We can then calculate the coverage for the $1 - \alpha$ level as $\sum_{i=1}^N \tilde{\alpha}_{\text{HPD}} \geq \alpha$, where N is the number of simulations.

A similar logic applies to DRP credibility regions. While we could find the radius from the reference point, such that α reaches a certain value, it is far more computationally efficient, and equivalent, to use the credibility regions defined by the true values, as shown in Fig. 7. This is the method used by Algorithm 2.

B. Intuition about over and under confident plots

Those used to applying coverage probabilities to validate SBI analysis, will be used to seeing over and underconfident curves, such as those in the blue curves of Fig. 2. However, the same figure shows how the DRP method gets different looking curves for over and underconfident posterior estimators. The aim of this appendix is to provide some intuition behind this.

Firstly, we focus on underconfident posteriors, shown in the top panel of Fig. 8. In this case, we see that the DRP coverage tends to be close to 0.5. This is because the DRP, independently of where the random reference point is, if the truth is close to the peak of the posterior, the DRP area is likely to cover approximately half of the distribution. On the other hand, for overconfident posteriors, shown in the bottom panel of Fig. 8, we see that the DRP coverage tends to be close to either 0 or 1. This is because the DRP, independently of where the random reference point is, if the truth is far from the peak of the posterior, the DRP area is likely to cover either the whole distribution, or none of it.

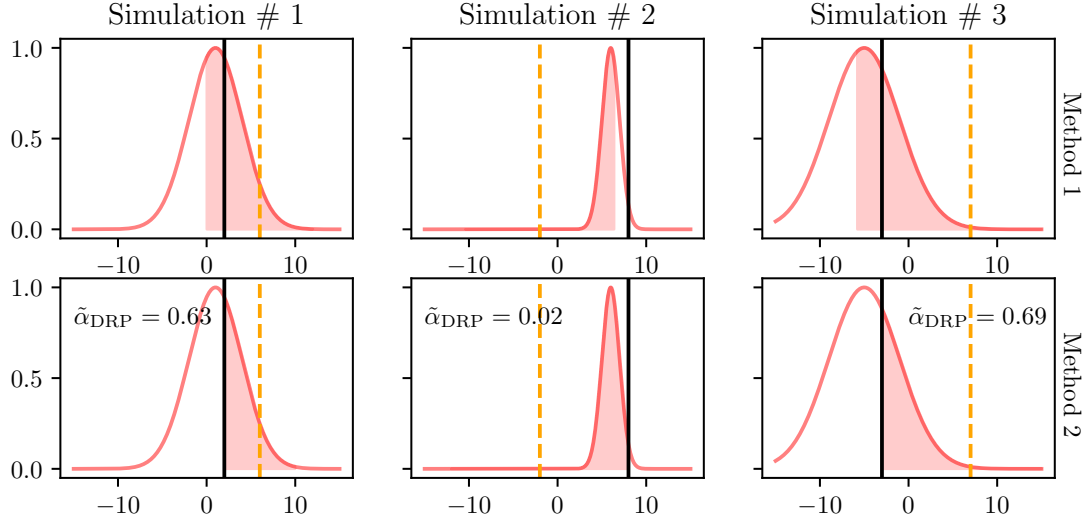


Figure 7. Similarly to Fig. 6, this figure illustrates the intuition behind the two ways of calculating ‘distance to random point’ coverages. Each column shows one of three simulations in a toy example. The red curves show the predicted posteriors, and the black vertical lines show the corresponding truths. The orange lines show the randomly selected reference points. We want to calculate the coverage for the 68% credibility level ($\alpha = 0.32$). The first approach, described in ??, shown in the top row, would consist of finding the $1 - \alpha$ credibility region centered around the reference point, then checking how often the truth is in said region (in this case twice, so the coverage is $2/3$). The alternative approach, shown in the bottom row, is to find the DRP region defined by the reference and the truth, then find how often $\tilde{\alpha}_{HPD} < \alpha$, which is again twice. The plot illustrates the fact that these two approaches are exactly equivalent.

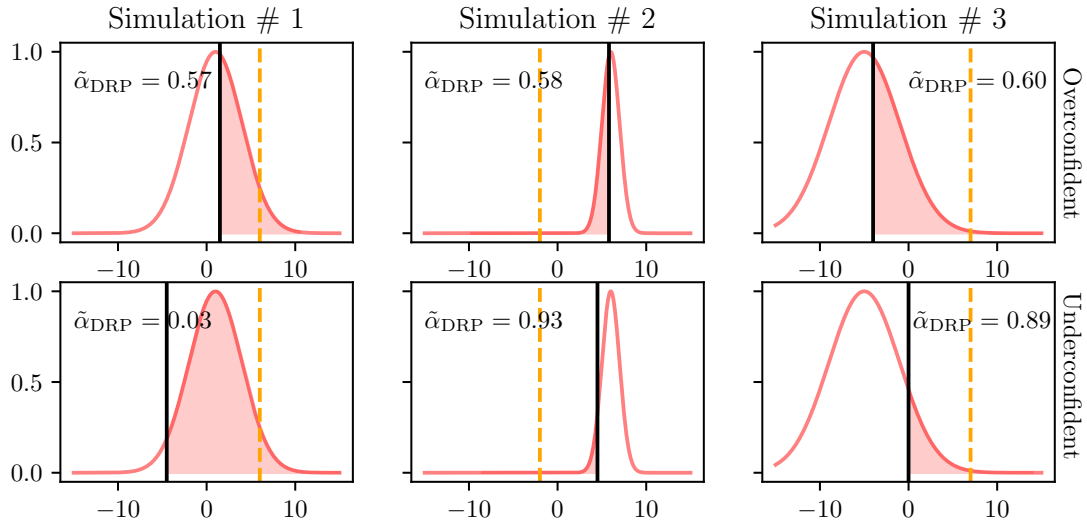


Figure 8. This figure illustrates the reason behind the shapes of over and underconfident curves obtained using DRP coverage, such as those in Fig. 2. The top shows three examples of overconfident predictions, while the bottom shows underconfident predictions. The figure shows that DRP coverages tend to be close to 0.5, while for overconfident regions they tend to be close to either 0 or 1.

C. Gravitational lensing experiment details

As shown in [Adam et al. \(2022\)](#), gravitational lensing source reconstruction can be performed using techniques from score-based modeling. Here we summarize the key ideas behind score-based modeling and how we generate biased and exact posterior samples.

Score-based modeling works by perturbing a training dataset sampled from a prior $p(\theta)$ with noise of increasing scales indexed by $t \in [0, T]$. Here $t = 0$ corresponds to unperturbed data ($p_0(\theta) = p(\theta)$) and $t = T$ corresponds to perturbing the data so much it is buried under noise and follows a Gaussian distribution ($p_T(\theta) = \mathcal{N}(\theta|0, \sigma_T^2)$). The noising process be described by the stochastic differential equation (SDE) ([Song et al., 2020](#))

$$d\theta_t = f(t, \theta) dt + g(t) dw, \quad (30)$$

where w is a standard Wiener process. Using denoising score-matching ([Hyvärinen & Dayan, 2005](#); [Vincent, 2011](#); [Song et al., 2020](#)), a neural network can be trained to approximate the time-dependent prior score $\nabla_\theta p_t(\theta)$, where $p_t(\theta)$ is the distribution over data perturbed by the noising process up to time t . Given the prior score, samples can be generated by solving the corresponding reverse SDE (RSDE) backwards in time, starting with samples from p_T :

$$d\theta = [f(t, \theta) - g^2(t) \nabla_\theta \log p_t(\theta)] dt + g(t) dw, \quad (31)$$

where here dt is a negative timestep.

For simplicity, instead of fitting a score-based model, we fit a multivariate Gaussian to the PROBES dataset of galaxy images as our prior, giving $p(\theta) = \mathcal{N}(\mu_0, \Sigma_0)$. We use the variance-exploding SDE from [Song et al. \(2020\)](#) as our noise process. The prior at time t is thus $p_t(\theta) = \mathcal{N}(\theta|\mu_0, \Sigma_0 + \sigma_t^2 \mathbb{I})$, where σ_t^2 is the variance of the noise process at time t . This expression can be used to evaluate the prior score analytically.

To modify the sampling procedure to generate samples from $p(\theta|x)$ for some observation x , we must condition the score in the RSDE, replacing the prior score with the posterior score:

$$d\theta = [f(t, \theta) - g^2(t) \nabla_\theta \log p_t(\theta|x)] dt + g(t) dw, \quad (32)$$

By Bayes' rule, the posterior score is

$$\nabla_\theta \log p_t(\theta|x) = \nabla_\theta \log p_t(x|\theta) + \nabla_\theta \log p_t(\theta), \quad (33)$$

where the first term on the RHS is the score of the likelihood. As pointed out in [Adam et al. \(2022\)](#), this time-dependent likelihood is in general intractable, but can be approximated as

$$\hat{p}_t(x|\theta) = \mathcal{N}(x|A\theta, \sigma_n^2 \mathbb{I} + \sigma_t^2 AA^T) \approx p_t(x|\theta), \quad (34)$$

where the matrix A encodes the lensing distortions and σ_n is the standard deviation of the noise in the observation (see § 4.3). *However*, when $p(\theta)$ is a multivariate Gaussian, the time-dependent likelihood is *tractable*, evaluating to

$$p_t(x|\theta) = \mathcal{N}(x|A\theta_c(\theta), \sigma_n^2 \mathbb{I} + A\Sigma_c A^T), \quad (35)$$

where

$$\Sigma_c := (\Sigma_0^{-1} + \sigma_t^{-2} \mathbb{I})^{-1}, \quad \theta_c(\theta) := \sigma_t^{-2} \Sigma_c \theta. \quad (36)$$

We therefore have two methods for sampling the posterior for the source galaxy's light: solving the RSDE (32) using the exact time-dependent likelihood ((35)) or the approximate, biased one ((34)). We refer to these as the ‘exact’ and ‘biased’ samplers respectively.

Finally, we solve both the exact and biased RSDEs by discretizing with the Euler-Maruyama method (see e.g. [Song et al. \(2020\)](#)). We find 300 steps is sufficient to ensure convergence.